Aquation of the Ruthenium-Based Anticancer Drug NAMI-A: A Density Functional Study

ARTICLE *in* THE JOURNAL OF PHYSICAL CHEMISTRY B · MAY 2008

Impact Factor: 3.3 · DOI: 10.1021/jp800411g · Source: PubMed

4 AUTHORS:

Neva Besker
Cineca
11 PUBLICATIONS **103** CITATIONS
SEE PROFILE

Cecilia Coletti
Università degli Studi G. d'Annunzio Chieti e …
56 PUBLICATIONS **721** CITATIONS
SEE PROFILE

Alessandro Marrone
Università degli Studi G. d'Annunzio Chieti e …
31 PUBLICATIONS **513** CITATIONS
SEE PROFILE

Nazzareno Re
Università degli Studi G. d'Annunzio Chieti e …
197 PUBLICATIONS **4,980** CITATIONS
SEE PROFILE

THE JOURNAL OF PHYSICAL CHEMISTRY B LETTERS

2008, *112,* 3871−3875
Published on Web 03/11/2008

Aquation of the Ruthenium-Based Anticancer Drug NAMI-A: A Density Functional Study

Neva Bešker, Cecilia Coletti, Alessandro Marrone, and Nazzareno Re*

Dipartimento di Scienze del Farmaco, Università degli Studi "G. D'Annunzio", I-66100 Chieti, Italy

Received: January 16, 2008; In Final Form: February 20, 2008

We carried out density functional theory (DFT) calculations to investigate the thermodynamics and the kinetics of the double aquation reaction of the anticancer drug NAMI-A. Three explicit water molecules were included in the calculations to improve the PB solvation energies. Our calculations show that the chloride substitution reactions on the considered Ru(III) octahedral complex follow a dissociative interchange mechanism, I_d, passing through a loose heptacoordinate transition state. We calculated an activation enthalpy and free energy for the first aquation step of 101.5 and 103.7 kJ mol^{-1}, respectively, values that are in good agreement with the available experimental results. The activation enthalpy and free energy for the second aquation step were found significantly higher, 118.7 and 125.0 kJ mol^{-1}, again in agreement with the experimental evidence indicating a slower rate for the second aquation.

Introduction

In attempts to find a new, metal-based anticancer drug with activity complementary to cisplatin, several ruthenium complexes have recently been investigated for their antitumor activity.[1−4] Among them, some ruthenium(III) complexes, designed on the model of cisplatin, have demonstrated favorable antitumor properties toward a number of in vitro and in vivo tumor models while showing lower systemic toxicity than platinum(II) compounds.[1−4]

In particular, Keppler-type complexes (HL)[*trans*-$RuCl_4L_2$] with L as a heterocyclic nitrogen ligand[5−7] and the related tetrachlororuthenium(III) dmso complexes of the type (X)[*trans*-$RuCl_4$(dmso-S)L] (L = imidazole; X = Na or HL, NAMI or NAMI-A, respectively)[8−9] have shown interesting antimetastatic properties. NAMI-A is the first ruthenium antitumor complex that has entered clinical testing and has recently successfully completed a phase I trial.[9c] The spectrum of the antitumor action of this complex differs significantly from that of cisplatin and presents an important antimetastatic rather than citotoxic activity.[8,9]

Although the mechanism of action of the NAMI-A-type complexes (HL)[*trans*-$RuCl_4$(dmso-S)L] is not yet understood, they appear to be prodrugs that hydrolyze rapidly in vivo, forming a number of potentially active species.[10−12] The investigation of the hydrolytic properties of this type of complex is therefore important for determining the nature of the active species and could be useful to optimize the protocols for the administration of the drugs.

NAMI-A is a hexacoordinate complex with pseudooctahedral geometry showing a square-planar arrangement of the four chlorides and the remaining dmso and imidazole ligands in the axial positions (Figure 1). In physiological conditions, it has been shown to undergo a hydrolysis reaction in which up to two chloride ligands are substituted by water leading to more reactive aquated species.[10−12]

A deeper insight into the aquation of NAMI-A is important to understand its mechanism of action in vivo and may be useful to design new ruthenium-based anticancer drugs. To this end, we carried out density functional theory (DFT) calculations to investigate the thermodynamics and the kinetics of NAMI-A aquation (see Scheme 1). Although ruthenium antitumor compounds have been the subject of intense experimental research, very few quantum mechanical studies have been performed, either at semiempirical level[13a] or on a specific organometallic ruthenium complex.[13b] While the manuscript was in preparation, a theoretical study, the first one to the best of our knowledge, on the hydrolysis of NAMI-A was published by Chen et al.[14] However, that study presented a disagreement between the calculated activation enthalpy for the second aquation step, lower than the value for the first aquation step, and the experimental evidence showing a slower rate for the second step[12] and attributed to the inaccuracy of the employed solvent model. Moreover, our study has been carried out at significantly higher level of theory: we performed geometry optimization and transition state search in solution, using also diffuse functions on both ruthenium and main group atoms, and considered three explicit water molecules to account more accurately for specific hydrogen bond interactions between the ruthenium ligands including the leaving chloride anion and the solvent.

Computational Details

All calculations were performed with the Jaguar 6.0 quantum chemistry package,[15] using density functional theory (DFT) with the B3LYP hybrid functional,[16] which is known to give good descriptions of reaction profiles for transition metal-containing compounds.[17] The 1s-4d core electrons of the ruthenium atom were described with the Hay and Wadt core-valence relativistic effective core potential (ECP),[18] leaving the outer electrons to be treated explicitly by a basis set of double-ζ quality plus one

* To whom correspondence should be addressed. E-mail: nre@unich.it. Tel.: +3908713554603. Fax: +3908713554614.

10.1021/jp800411g CCC: $40.75

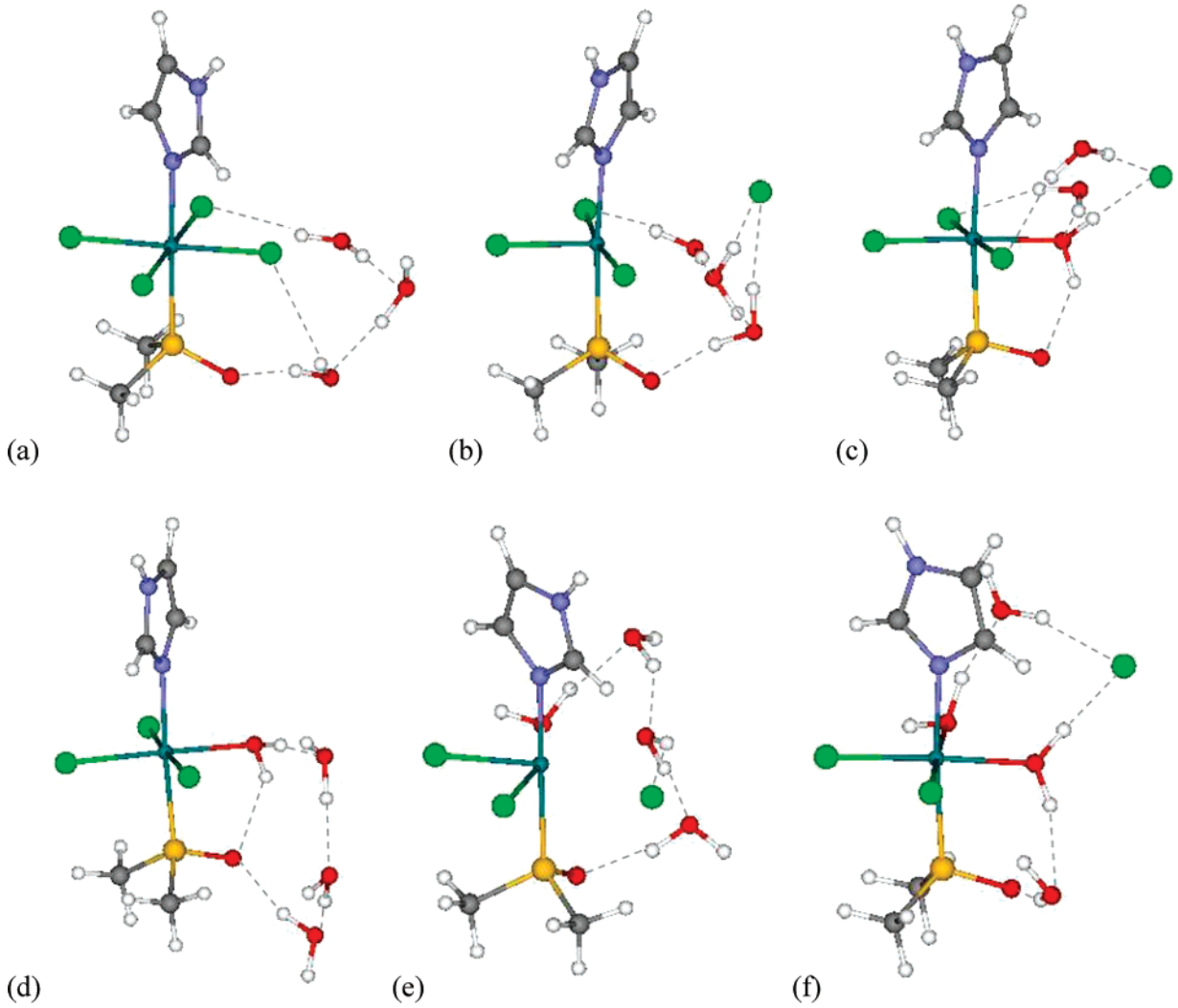

Figure 1. Geometries of the reagents, transition states and products of the two aquation steps of NAMI-A: (a) R1, (b) TS1, (c) P1, (d) R2, (e) TS2, and (f) P2.

SCHEME 1: Proposed First and Second Aquation Processes for NAMI-A

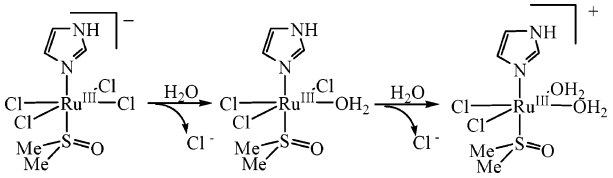

diffuse d function and two polarization sp functions, while all electrons were considered for remaining atoms with the 6-31G+(d,p) basis set[19] (denoted as LACVP+** in Jaguar). Every structure in its doublet state was optimized by unrestricted calculations in gas phase and in solution, using the Poisson−Boltzmann (PB) continuum solvent method to simulate the aqueous environment.[20] Frequency calculations were performed to verify the correct nature of the stationary points and to estimate zero-point energy (ZPE) and vibrational entropy corrections at room temperature. Intrinsic reaction coordinate (IRC) calculations were employed to correctly locate reagents and products. The energies of all stationary points have been reevaluated with single point calculations using the larger LACV3P++**, consisting of the 6-311++G(d,p) set for the main group elements,[21] and of the Hay and Wadt core valence ECP basis set of triple-ζ quality plus one diffuse d function and two polarization sp functions for the metal atom.[20]

Results and Discussion

The NAMI-A complex was modeled considering the [*trans*-$RuCl_4$(dmso-S)(Im)]$^-$ anion. The minimized structure of this isolated anion matches the crystallographic data accurately with bond distances within 0.1 Å and bond angles within 3°[22] (see Supporting Information, Table S1) thus indicating that the B3LYP provides a good description of the molecular structures of these systems. According to experimental and theoretical studies, ligand substitution reactions on a Ru(III) octahedral complex are accepted to follow associative to dissociative interchange mechanisms, I_a or I_d, passing through a hepta-coordinate transition state.[23] We investigated the aquation reaction using a model in which three water molecules were included to incorporate the effect of specific hydrogen bonding and to provide a more accurate description of the hydration of the leaving chloride anion. For the first aquation step, the three water molecules were placed in the reaction hemisphere of the [*trans*-$RuCl_4$(dmso-S)(Im)]$^-$ anion. For the second aquation step, the first leaving chloride anion was removed and the water molecules were placed in the reaction hemisphere of the monoaquated neutral [*trans*-$RuCl_3(H_2O)$(dmso-S)(Im)] species. The three water molecules were initially located in the second coordination sphere around the leaving chloride ligand in such a way to form hydrogen bonds with the dmso oxygen and the neighbor chloride or aquo ligands. Both aquation steps were

TABLE 1: Main Geometrical Parameters Calculated for Reagents, Transition States, and Products of the Two Aquation Steps of NAMI-A[a]

	first aquation			second aquation		
	R1	TS1	P1	R2	TS2	P2
Ru-Cl1	2.387	3.923	4.608			
Ru-Cl2	2.413	2.362	2.406	2.395	3.048	4.539
Ru-Cl3	2.421	2.303	2.369	2.367	2.378	2.367
Ru-Cl4	2.426	2.376	2.403	2.397	2.378	2.362
Ru−O(w1)	4.506	3.225	2.141	2.169	2.251	2.142
Ru−O(w2)				4.749	2.508	2.097
Ru−S	2.447	2.464	2.413	2.454	2.460	2.447
Ru−N	2.109	2.100	2.109	2.102	2.103	2.094
Cl1-Ru-Cl2	89.1	75.3				
Cl1-Ru-Cl3	178.7	156.3				
Cl1-Ru-Cl4	89.9	96.1				
Cl2-Ru-Cl3	90.7	94.7	91.2	92.6	72.7	90.9
Cl2-Ru-Cl4	179.1	171.1	177.8	172.5	156.9	112.0
Cl3-Ru-Cl4	90.1	94.2	91.1	94.8	84.2	95.0
Cl4-Ru−N	89.4	89.6	90.2	91.4	90.6	93.5
Cl4-Ru−S	89.4	93.2	91.1	89.5	91.0	91.4
N−Ru−S	178.2	174.9	174.6	177.6	177.4	174.6
O(w1)-Ru-Cl2	133.4	100.2	90.0	87.3	126.2	63.9
O(w1)-Ru-Cl3	134.0	154.3	176.9	176.6	161.0	175.7
O(w1)-Ru-Cl4	45.8	71.8	88.8	85.2	76.8	88.4
O(w2)-Ru−O(w1)					65.6	85.9
O(w2)-Ru-Cl3					133.3	90.9
O(w2)-Ru-Cl4					142.1	172.6

[a] Cl1 and Cl2 are the chloride anions leaving, respectively, in the first and second aquation steps, while w1 and w2 are the corresponding entering water molecules (see Figure 1). Cl3 and Cl4 are numbered anticlockwisely in the equatorial plane.

assumed to proceed from these reactant clusters, R, to the corresponding products in which the chloride anion remains in the second coordination sphere, P, via a heptacoordinate transition state

$$[RuCl_4(dmso)(Im)]^-\cdot(H_2O)_3\ (R1) \rightarrow \{[RuCl_3(dmso)(Im)\cdots(H_2O)(Cl^-)]\cdot(H_2O)_2\}^{\ddagger}\ (TS1) \rightarrow [RuCl_3(H_2O)(dmso)(Im)]\cdot(H_2O)_2(Cl^-)\ (P1)$$

$$[RuCl_3(H_2O)(dmso)(Im)]\cdot(H_2O)_3\ (R2) \rightarrow \{[RuCl_2(H_2O)(dmso)(Im)^+\cdots(H_2O)(Cl^-)]\cdot(H_2O)_2\}^{\ddagger}\ (TS2) \rightarrow [RuCl_2(H_2O)_2(dmso)(Im)]^+\cdot(H_2O)_2(Cl^-)\ (P2)$$

Both cis and trans isomers were considered for the diaquo complex $[RuCl_2(H_2O)_2(dmso)(Im)]^+$.

1. Geometry Structures. Optimizations have been performed both in gas phase and in solution, and because the results are very close only the values in solution will be discussed. Although several local minima could be found for reagents and products, differing by few kJ mol^{-1}, in the following we only discuss those correlated to the transitions states, obtained by IRC calculations. Figure 1 displays the optimized stationary points for the two hydration steps while the main geometrical parameters are presented in Table 1. In the optimized reagent structure of the first aquation step, R1, the three explicit water molecules form a tight interconnected hydrogen bond network with one water interacting with the oxygen atom of dmso and the remaining two waters with two adjacent chloride ligands. In the transition structure, TS1, the entering water molecule approaches the metal center with the Ru−O distance decreasing from 4.506 to 3.225 Å, as the adjacent leaving chloride anion moves further with the Ru−Cl distance increasing from 2.387 to 3.923 Å, indicating an interchange dissociative rather than associative character of the transition state. In the optimized product structure P1, the entering water has replaced the chloride ligand, which has moved far away from the metal center, as shown by the Ru−O = 2.141 Å and Ru−Cl = 4.608 Å distances. In both TS1 and P1, the leaving chloride anion is close to the two remaining explicit water molecules in the second coordination sphere attracting their positively charged hydrogen atoms and can thus be considered as partially solvated.

The optimized stationary points for the second aquation step are quite similar to those for the first step and show essentially the same hydrogen bond pattern. In R2, the three explicit water molecules form again a stable hydrogen bond network where one of them interacts more strongly with the aquo ligand adjacent to the leaving chloride. In the transition state TS2, the Ru−O and Ru−Cl distances, respectively 2.508 and 3.048 Å, are significantly shorter than in TS1 in agreement with the positive charge in the former species. In the optimized product P2, the entering water has replaced the second chloride ligand, as shown by the Ru−O = 2.097 Å and Ru−Cl = 4.539 Å distances. Again, in both TS2 and P2 the leaving chloride anion is partially solvated by the two remaining explicit water molecules in the second coordination sphere.

2. Energy Profiles. In Table 2 we give the calculated relative electronic energies, enthalpies, and free energies of the stationary points in both gas phase and in solution, along with their solvation energies, entropies, and thermal corrections. Two sets of data are reported for the values in solution, that is, those obtained from single point calculations on the gas-phase geometries and those obtained upon optimization in solution phase. Because the three explicit water molecules partially account for solvation effects, the activation and reaction energies in gas phase are close to those in solution. Moreover, Table 2 shows that the optimization calculations in solution have a significative influence on the activation enthalpies and free energies. This result is consistent with a large body of theoretical calculations on water exchange reactions in octahedral complexes, showing that optimization in solution is required for a quantitative reproduction of the experimental activation and reaction energies.[23] Gas phase and subsequent single point calculations in solution indicate activation and reaction enthalpies and free energies for the second aquation path leading to the *trans* isomer much larger than the corresponding values for the *cis* isomer, $\Delta H^{\ddagger}$ = 145.6 versus 115.3 kJ mol^{-1} $\Delta G^{\ddagger}$ = 152.7 versus 121.6 kJ mol^{-1} and ΔH = 43.5 versus 19.6 kJ mol^{-1} ΔG = 40.2 versus 23.8 kJ mol^{-1} in solution; therefore only the cis isomer will be discussed below. Figure 2 and 3 display, respectively, the enthalpy and free energy profiles for the two aquation steps using the values obtained from the more reliable optimization in solution phase. It can be noted that the values of activation and reaction free energies are very close to the corresponding enthalpies (within 2 and 6 kJ mol^{-1}, respectively, for the first and second aquation). The activation enthalpy and free energy for the first aquation step are 101.5 and 103.7 kJ mol^{-1}, respectively, values that are in good agreement with the experimentally determined rate constants for the degradation of NAMI.[10] Indeed, the use of Eyring equation,[24] through the calculated activation free energy value, gives an estimate of the rate constant for the first aquation process of 3.9×10^{-6} s^{-1}, which compares very well with the experimental results ranging from 1.4×10^{-7} to 3.1×10^{-6} at $7 < pH < 10$,[10a] and 5.58×10^{-6} s^{-1} in phosphate buffer at pH = 7.4.[10b] The activation enthalpy and free energy for the second aquation step are 118.7 and 125.0 kJ mol^{-1}, respectively, significantly higher than those for the first step, again in agreement with the experimental evidence indicating a slower

TABLE 2: Electronic Energies, ZPE-Corrected Energies, Enthalpies, Free Energies, Solvation Free Energies (all in kJ mol^{-1}) and Entropies (J mol^{-1} K^{-1}) Calculated for Reagents, Transition States and Products of the Two Aquation Steps of NAMI-A

	first aquation								
	gas phase			solution (single point)			solution (optimized)		
	R1	TS1	P1	R1	TS1	P1	R1	TS1	P1
ΔE	0	121.2	17.1	0	122.5	22.1	0	104.9	−1.3
ΔE^{ZPE}	0	119.4	16.7	0	120.7	21.7	0	103.0	−1.8
ΔH	0	117.8	15.9	0	119.1	20.9	0	101.5	−2.5
ΔG	0	120.0	16.3	0	121.3	21.3	0	103.7	−2.1
S	182.7	180.7	182.5	182.7	180.7	182.5	182.7	180.7	182.5
Gsolv				−290	−289	−286	−335	−349	−345
	second aquation								
	gas phase			solution (single point)			solution (optimized)		
	R2	TS2	P2	R2	TS2	P2	R2	TS2	P2
ΔE	0	129.5	41.3	0	118.3	27.1	0	121.6	17.5
ΔE^{ZPE}	0	128.5	36.7	0	117.3	22.5	0	120.6	12.9
ΔH	0	126.6	33.8	0	115.3	19.6	0	118.7	10.0
ΔG	0	132.9	38.0	0	121.6	23.8	0	125.0	14.2
S	183.4	178.2	179.8	183.4	178.2	179.8	183.4	178.2	179.8
Gsolv				−132	−144	−147	−154	−155	−212

rate for the second aquation step, although a quantitative estimate of the energy barrier is not available.[12] Moreover, while the first aquation step was predicted to be slightly exothermic by 2.5 kJ mol^{-1}, the second step was found slightly endothermic by 10 kJ mol^{-1}, indicating that the latter step is also thermodynamically unfavored.

A comparison of our results with those of Chen et al.[14] is not straightforward due to the different models employed to account for solvation. Indeed, because our model includes three explicit water molecules in vacuo, which partially account for solvation, a direct comparison is possible only after the complete inclusion of the solvation effects through a polarized continuum model, PB for our calculations and PCM for those in ref 14. A reasonable agreement is observed for the activation and reaction enthalpies and free energies in solution of the first aquation step within 2−3 kcal mol^{-1}, and the values obtained in ref 14 for the second aquation step are significantly lower than our results (by 6−7 kcal mol^{-1}). However, the activation and reaction

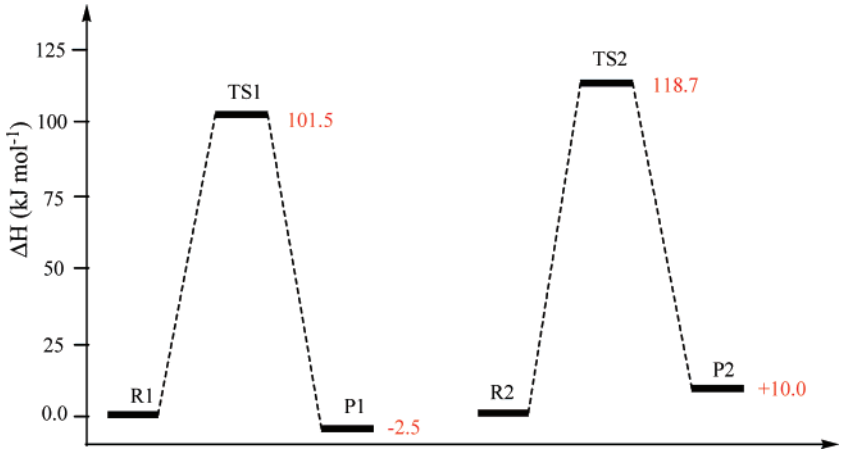

Figure 2. Enthalpy profile for the first and second aquation steps of NAMI-A.

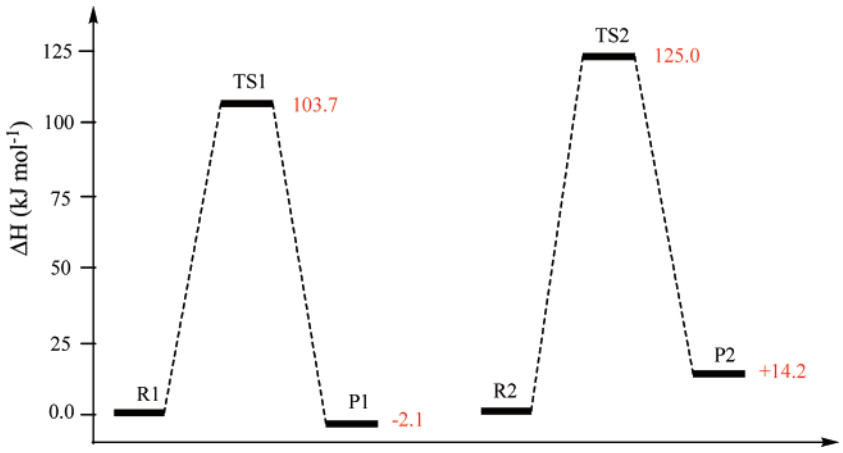

Figure 3. Free Energy profile for the first and second aquation steps of NAMI-A.

enthalpies and free energies calculated for the second aquation step in ref 14 are even lower than those for the first aquation step and indeed in disagreement with the experimental evidence clearly showing that the second aquation step has a slower rate than the first one. Because we employed the same hybrid B3LYP exchange-correlation potential and a basis set larger by only a diffuse function on the metal and main group atoms in our calculations, we attribute these differences mainly to the better simulation of solvation both through the inclusion of explicit water molecules and the use of the more accurate PB continuum model.

Conclusion

In this work, we have performed a complete mechanistic study of the double aquation reaction of the anticancer drug NAMI-A by using hybrid DFT methods. Geometries and vibrational frequencies were obtained at the B3LYP/6-31+G(d,p) level (employing the relativistic Los Alamos pseudopotential for the ruthenium atom) both in gas phase and in aqueous solution, followed by single point energy calculations at B3LYP/6-311++G(d,p) level. Three explicit water molecules were included in the calculations to improve the PB solvation energies. Our calculations show that the chloride substitution reactions on the considered Ru(III) octahedral complex follow a dissociative interchange mechanism, I_d, passing through a loose heptacoordinate transition state. We calculated an activation enthalpy and free energy for the first aquation step of 101.5 and 103.7 kJ mol^{-1}, respectively, values that are in good agreement with the available experimental results, while the activation enthalpy and free energy for the second aquation step were found significantly higher, 118.7 and 125.0 kJ mol^{-1}, again in agreement with the experimental evidence indicating a slower rate for the second aquation.

Acknowledgment. Italian Ministry for University and Research is acknowledged for financial support (contract 2006038520)

Supporting Information Available: A table with the comparison between the calculated and the X-ray geometries for NAMI-A and NAMI and the Cartesian coordinates for all the optimized geometries. This material is available free of charge via the Internet at http://pubs.acs.org.

References and Notes

(1) (a) Keppler, B. K. In *Progress in Clinical Biochemistry and Medicine*; Springer: Berlin, 1989; Vol. 10, p 41. (b) Clarke, M. J. In *Metal Complexes in Cancer Chemotherapy*; Keppler, B. K., Ed.; VCH: Weinheim, 1993; p 129. (c) Keppler, B. K., Lipponer, K. G., Stenzel, B.; Kratz, F. In *Metal Complexes in Cancer Chemotherapy*; Keppler, B. K., Ed.; VCH: Weinheim, 1993; pp 187−220. (d) Clarke, M. J.; Zu, F.; Frasca, D. R. *Chem. Rev.* **1999**, *99*, 2511−2533. (e) Clarke, M. J. *Coordination Chem. Rev.* **2002**, *232*, 69−93.

(2) (a) Ang, W. H.; Dyson, P. J. *Eur. J. Inorg. Chem.* **2006**, 4003−4018. (b) Brabec, V.; Novakova, O. *Drug Resist. Update* **2006**, *9*, 111−122.

(3) (a) Reedijk, J. *Proc. Natl. Acad. Sci. U.S.A.* **2003**, *100*, 3611. (b) Allardyce, C. S.; Dyson, P. J.; *Platinum Met. Rev.* **2001**, *45*, 62−69.

(4) Frasca, D.; Ciampa, J.; Emerson, J.; Umans, R. S.; Clarke, M. J. *Met.-Based Drugs* **1996**, *3*, 197−209.

(5) Galanski, M.; Arion, V. B.; Jakupec, M. A.; Keppler, B. K. *Curr. Pharm. Des.* **2003**, *9*, 2078−2089.

(6) (a) Hartinger, C. G.; Zorbas-Seifried, S.; Jakupec, M. A.; Kynast, B.; Zorbas, H.; Keppler, B. K. *J. Inorg. Biochem.* **2006**, *100*, 891−904. (b) Jakupec, M. A.; Arion, V. B.; Kapitza, S.; Reisner, V; Eichinger, A.; Pongratz, M.; Marian, B.; Graf, N.; Keyserlingk, V.; Keppler, B. K. *Int. J. Clin. Pharmacol. Ther.* **2005**, *43*, 595−596.

(7) Kapitza, S.; Pongratz, M.; Jacupec, M. A.; Heffeter, P.; Berger, W.; Lackinger, L.; Keppler, B. K.; Marian, B. *J. Cancer Res. Clin. Oncol.* **2005**, *131*, 101−110.

(8) Sava, G.; Pacor, S.; Mestroni, G.; Alessio, E. *Anti-Cancer Drugs* **1992**, *3*, 25−31.

(9) (a) Sava, G.; Gagliardi, R.; Bergamo, A.; Alessio, E.; Mestroni, G. *Anticancer Res.* **1999**, *19*, 969−972. (b) Alessio, E.; Mestroni, G.; Bergamo, A.; Sava, G. *Curr. Top. Med. Chem.* **2004**, *4*, 1525−1535. (c) Rademaker-Lakhai, J. M.; Van Den Bongard, D.; Pluim, D.; Beijnen, J. H.; Schellens, J. H. M. *Clin. Cancer Res.* **2004**, *10*, 3717−3727.

(10) (a) Bouma, M.; Nuijen, B.; Jansen, M. T.; Sava, G.; Flaibani, A.; Bult, A.; Beijnen, J. H. *Int. J. Pharm.* **2002**, *248*, 239−246. (b) Bouma, M.; Nuijen, B.; Jansen, M. T.; Sava, G.; Flaibani, A.; Bult, A.; Beijnen, J. H. *J. Pharm. Biomed. Anal.* **2002**, *30*, 1287−1296.

(11) Mestroni, G.; Alessio, E.; Sava, G.; Pacor, S.; Coluccia, M.; Bocarelli, A. *Met.-Based Drugs* **1994**, *1*, 41−63.

(12) Sava, G.; Bergamo, A.; Zorzet, S.; Gava, B.; Casarsa, C.; Cocchietto, M.; Furlani, A.; Scarcia, V.; Serli, B.; Iengo, E.; Alessio, E.; Mestroni, G. *Eur. J. Cancer* **2002**, *38*, 427−435.

(13) (a) Chen, J. C.; Li, J.; Qian, L.; Zheng, K. C. *J. Mol. Struct. (THEOCHEM)* **2005**, *728*, 93−101. (b) Scolaro, C.; Geldbach, T. J.; Rochat, S.; Dorcier, A.; Gossens, C.; Bergamo, A.; Cocchietto, M.; Tavernelli, I.; Sava, G.; Rothlisberger, U.; Dyson, P. J. *Organometallics* **2006**, *25*, 756−765.

(14) Chen, J.; Chen, L.; Liao, S.; Zheng, K.; Ji, L. *J. Phys. Chem B* **2007**, *111*, 7862−7869.

(15) *Jaguar 6.0*; Schrodinger, LLC: New York, 2005.

(16) (a) Becke, A. D. *J. Chem. Phys.* **1993**, *98*, 5648−5652. (b) Becke, A. D. *Phys. Rev. A* **1988**, *38*, 3098−3100.

(17) (a) Niu, S.; Hall, B. M. *Chem. Rev.* **2000**, *100*, 353. (b) Nielsen, R. J.; Keith, J. M.; Stoltz, B. M.; Goddard, W. A., III *J. Am. Chem. Soc.* **2004**, *126*, 7967−7974.

(18) Hay, P. J.; Wadt, W. R. *J. Chem. Phys.* **1985**, *82*, 299−310.

(19) Hariharan, P. C.; Pople, J. A. *Chem. Phys. Lett.* **1972**, *16*, 217−219.

(20) Tannor, D. J.; Marten, B.; Murphy, R.; Friesner, R. A.; Sitkoff, D.; Nicholls, A.; Ringnalda, M.; Goddard, W. A., III; Honig, B. *J. Am. Chem. Soc.* **1994**, *116*, 11875−11882.

(21) McLean, A. D.; Chandler, G. S. *J. Chem. Phys.* **1980**, *72*, 5639−5648.

(22) Alessio, E.; Balducci, G.; Lutman, A.; Mestroni, G.; Calligaris, M.; Attia, W. M. *Inorg. Chim. Acta*. **1993**, *203*, 205−217.

(23) (a) Rotzinger, F. P. *Chem. Rev.* **2005**, *105*, 2003−2037 and references therein. (b) Rotzinger, F. P. *J. Phys. Chem B* **2005**, *109*, 1510−7869. (c) Aebischer, N.; Sidorenkova, E.; Ravera, M.; Laurenczy, G.; Osella, D.; Weber, J.; Merbach, A. E. *Inorg. Chem.* **1997**, *36*, 6009−6020.

(24) We used the Eyring equation in the form: $k = (k_B T/h)\exp(-\Delta G^{\ddagger}/RT)$, where k_B is the Boltzmann constant, T is the absolute temperature, h is the Planck constant, and $\Delta G^{\ddagger}$ is the activation free energy.